Electron-Stimulated Production of Molecular Oxygen in Amorphous Solid Water

Nikolay G. Petrik, Alexander G. Kavetsky,† and Greg A. Kimmel*

Fundamental Sciences Directorate, Pacific Northwest National Laboratory, Mail Stop K8-88, P.O. Box 999, Richland, Washington 99352

Received: September 13, 2005; In Final Form: November 15, 2005

The low-energy, electron-stimulated production of molecular oxygen from pure amorphous solid water (ASW) films and ASW films codosed with H_2O_2 is investigated. Layered films of $H_2{}^{16}O$ and $H_2{}^{18}O$ are used to investigate the reaction mechanisms for O_2 production and the spatial profile of the reactions within the films. The O_2 yield is dose-dependent, indicating that precursors are involved in the O_2 production. For temperatures below ∼80 K, the O_2 yield at steady state is relatively low and nearly independent of temperature. At higher temperatures, the yield increases rapidly. The O_2 yield is enhanced from H_2O_2-dosed water films, but the experiments show that H_2O_2 is not the final precursor in the reactions leading to O_2. Instead, a stable precursor for O_2 is produced through a multistep reaction sequence probably involving the reactions of OH radicals to produce H_2O_2 and then HO_2. The O_2 is produced in a nonthermal reaction from the HO_2. For relatively thick films, the reactions leading to O_2 occur at or near the ASW/vacuum interface. However, the electronic excitations that initiate the reactions occur over a larger range in the film. A kinetic model that qualitatively accounts for all of the observations is presented.

I. Introduction

The fundamental mechanisms of the radiolytic decomposition of condensed water and aqueous solutions are of considerable interest to a number of fields, including radiation biology and medicine, nuclear energy and technology, and planetary sciences. Because the interaction of high-energy radiation with water produces numerous low-energy secondary electrons, the subsequent reactions of these electrons are particularly important. The general mechanisms of electron-driven processes in homogeneous, dilute aqueous systems have been characterized in research over the last several decades.[1] More recently, the interactions of electrons,[2−7] photons,[8,9] and ions[10] with condensed water have been extensively studied and a variety of nonthermal reaction mechanisms have been identified. However, a detailed molecular-level understanding of the relevant physical and chemical processes has yet to emerge.

Orlando and co-workers have previously investigated the electron-stimulated production of O_2 in ASW films in the temperature range from ∼90−150 K.[11,12] Their main conclusions regarding the mechanisms of O_2 formation were that: (1) the energetic threshold for O_2 electron-stimulated desorption (ESD) is ∼10 eV and the yield increases monotonically with energy up to at least 100 eV, indicating that ionization is the first step in the O_2 ESD, (2) the energetic electrons produce a stable precursor in the ASW films by a single nonthermal reaction, (3) the precursor is probably H_2O_2 or HO_2, and (4) the O_2 is produced by a second electronic excitation that directly dissociates the precursor molecule. In their model, the temperature dependence of the O_2 production arises from temperature-dependent changes in the lifetime of the electronic excitations responsible for the first step in the mechanism. Their results are in contrast to earlier models, which proposed that the O_2 is produced by the diffusion and subsequent reaction of radicals (such as OH) produced within the film by energetic particles (e.g., electrons, ions, or photons).[10,13,14] However, it is important to note that the minimum temperature for the ESD experiments of Orlando and co-workers (∼90 K) was above the temperature (∼80 K) where earlier experiments had found that the O_2 yield vs temperature began increasing.

Here, we investigate the low-energy, electron-stimulated production of O_2 in pure ASW films and ASW films codosed with H_2O_2 deposited on Pt(111) in the temperature range from 20 to 130 K. The data indicate that O_2 results from reactions involving OH radicals to produce H_2O_2 and then HO_2. The O_2 is then produced from the HO_2, which is a stable precursor, by a nonthermal reaction. Layered films of $H_2{}^{16}O$ and $H_2{}^{18}O$ were used to investigate the spatial profile of the nonthermal reactions in the ASW films. The results show that the O_2 is produced at or near the vacuum interface, even though ionizations and excitations deeper within the film contribute to the reactions near the vacuum interface. A kinetic model is presented that qualitatively reproduces all of the experimental results.

The rest of the paper is organized as follows: Section II describes the experimental apparatus and procedures. Section III presents the experimental results. The proposed reaction scheme for the electron-stimulated production of O_2 is given in Section IV, part A. The kinetic model is described and compared to the data in Section IV, part B, and finally the results are summarized in Section V.

II. Experimental Section

The experiments were performed in an ultrahigh vacuum (UHV) system, equipped with a low-energy electron gun (Kimball Physics ELG-2), a closed-cycle helium cryostat (Advanced Research Systems CSW 204B), a molecular beamline for growing thin films of water, an Auger electron spectrometer, and a quadrupole mass spectrometer (QMS) with an integrating cup.[15] Typical base pressures for the system were

* Corresponding author. E-mail: gregory.kimmel@pnl.gov.
† Current address: Khlopin Radium Institute, 28, 2nd Murinsky Street, St. Petersburg, Russia.

10.1021/jp055173v CCC: $33.50 © 2006 American Chemical Society
Published on Web 01/19/2006

$\sim 1 \times 10^{-10}$ Torr. The polished platinum single crystal was 10 mm in diameter, 1 mm thick, and was cut to within $\pm 0.5°$ of the (111) surface orientation. The Pt(111) was cleaned by neon ion sputtering and annealing at 1050 K in vacuum. The sample was resistively heated, and the temperature was measured with a K-type thermocouple spot-welded to the rear side of the sample.

The ASW films were deposited with the molecular beam at normal incidence to the Pt(111) under conditions known to produce dense, relatively smooth ASW.[16−18] The ASW films were smaller than, and centered on, the sample. To calibrate the water coverage, θ, we used the area of the first monolayer (ML) peak in the temperature-programmed desorption (TPD) spectra. The estimated absolute uncertainty in the coverages is $\pm 15\%$. The relative coverages are reproducible to $\pm 2\%$ between different experiments.

For H_2O_2 deposition, we used a commercial 50 wt % ($\sim$35 mol %) water solution from Aldrich. The solution was concentrated by extended distillation until the total vapor pressure over the solution was 3−4 Torr (at 20 °C), which should correspond to 70−80 mol % H_2O_2 in solution and $\sim$30 mol % in vapor phase.[19] However, reactions of the H_2O_2 with the walls of the gas manifold reduce the pressure of H_2O_2 by a factor of $\sim$10 such that the H_2O_2 pressure is $\sim$1% in the vapor phase. The decomposition of the H_2O_2 creates some O_2 in the gas manifold, which is difficult to control. The O_2 in the manifold was minimized by periodic evacuations of the headspace. However, for film growth temperatures above 40 K, O_2 does not adsorb on the water films, and therefore, the H_2O_2 predosed films described below were not contaminated with predosed O_2.

The ASW films were irradiated with 87 eV electrons with typical instantaneous current densities of $\sim 2 \times 10^{15}$ electrons/cm^2 s and beam spot sizes of $\sim$1.5 mm. Some experiments were performed over a wider current density range (i.e., $\sim 1 \times 10^{13}$ to 2×10^{15} electrons/cm^2 s). The electron beam was incident at 35° to the sample normal. The ASW films were uniformly irradiated by repeatedly scanning the electron beam in a grid pattern (typically with more than 1000 pixels at $\sim$1 ms/pixel) over an area slightly larger than the film. For each scan of the film, an average ESD signal is generated by sampling the output from the QMS several hundred times for each pixel in the scan and then averaging these values for the entire scan. The scan-averaging mode significantly improves the signal-to-noise ratio in comparison to irradiation of a single point in the film.

III. Results

The O_2 ESD signals vs irradiation time from 70 ML D_2O films are shown for temperatures ranging from 20 to 130 K in Figure 1. All the D_2O films were grown at 100 K and at normal incidence, conditions that produce dense, relatively smooth ASW films.[17,18] Therefore, the initial structure of the film is the same in all cases. In general, the O_2 ESD increases with increasing temperature. At all temperatures, the O_2 ESD signal is initially approximately zero and then increases until reaching a steady-state value. At the end of the electron irradiation, the O_2 ESD signal promptly decays to zero independent of the temperature (Figure 1b). For $T > \sim 80$ K, the O_2 ESD signal increases in time as $\sim(1 - e^{-\alpha t})$, while for lower temperatures, the dose dependence is more complicated. When normalized by the incident electron current density, the O_2 ESD vs electron dose is approximately independent of the incident electron current density over a fairly wide range (data not shown). For all irradiation temperatures, if after some delay time (up to several hours) the films are irradiated a second time, the O_2 ESD signal promptly returns to the level obtained at the end of the first irradiation cycle, in agreement with earlier observations.[11,12] Because the initial O_2 ESD yield is zero, increases with electron dose, and promptly recovers after a long interruption, the O_2 is produced from a stable precursor that accumulates in the film with increasing electron dose.

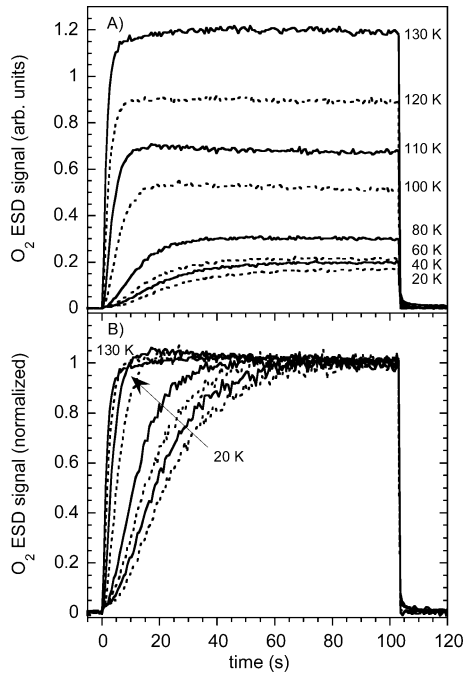

Figure 1. O_2 electron-stimulated desorption vs time. The 70 ML amorphous D_2O films were deposited at 100 K and then irradiated at various temperatures with 87 eV electrons. (A) Raw data (not normalized). At all temperatures, the O_2 ESD yield is initially zero and then saturates at longer irradiation times. (B) Same as (A), except normalized by the O_2 ESD yield at saturation.

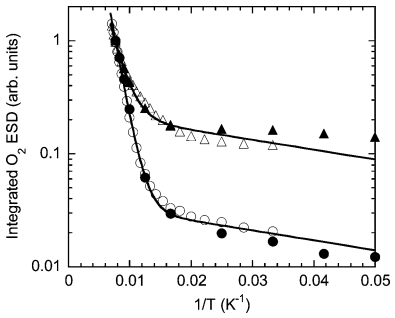

Figure 2. Integrated O_2 electron-stimulated desorption yield vs inverse temperature from amorphous D_2O. The O_2 yields have been normalized at high temperatures. For both the initial part of the irradiation (circles) and at saturation (triangles), the integrated O_2 ESD yield decreases as the inverse temperature increases. The results for thinner (30 ML, open symbols) and thicker (70 ML, solid symbols) films are similar. The solid lines are double exponential fits to the data.

The integrated O_2 ESD yield as a function of inverse temperature is shown in Figure 2. The figure shows the integrated yield at long times after the O_2 signal has saturated, as well as the integrated yield at the beginning of the irradiation. For both cases, the O_2 yield gradually increases until $\sim$80 K and then more rapidly at higher temperatures. The integrated O_2 ESD yields can be reasonably well fit with a double exponential with apparent activation energies of $\sim$0.05−0.06 eV and $\sim$0.002 eV. Note that the apparent change in O_2 ESD kinetics at $\sim$80 K (Figure 1b) corresponds to where the temperature dependence of the yield changes. For $T > 80$ K, the results in Figures 1 and 2 are in agreement with earlier

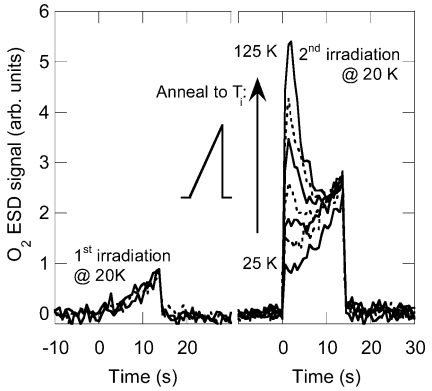

Figure 3. O_2 electron-stimulated desorption vs time. D_2O films (100 ML) deposited at 100 K were irradiated at 20 K for 15 s (left panel), annealed to various temperatures (25, 60, 80, 90, 100, 110, and 125 K) with a linear temperature ramp of 0.5 K/s, and then irradiated a second time at 20 K (right panel). For the second irradiation, the initial O_2 ESD yield increases with annealing temperature, demonstrating that precursors accumulate in the irradiated film that can subsequently react thermally to produce the final precursor for the O_2 ESD.

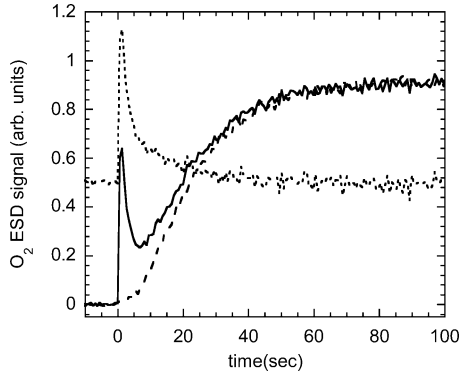

Figure 4. O_2 electron-stimulated desorption vs time for 60 ML D_2O films irradiated at 20 K. For a film irradiated at 20 K (dashed line), the O_2 ESD is initially zero. For a film initially irradiated at 100 K, cooled to 20 K, and then irradiated a second time (solid line), the initial O_2 ESD signal is large, quickly decays, and then tracks the data for the film initially irradiated at 20 K. The difference between the two curves (dotted line) decays approximately exponentially (offset for clarity).

reports.[11,12] However, the dose dependence of the ESD yield at lower temperatures suggests that the O_2 precursor is not produced directly by a nonthermal reaction, but is itself the product of a reaction (or reactions) between some other precursors.

To test the idea that the final O_2 precursor is not produced directly by the energetic electrons, we investigated the O_2 ESD in water films irradiated twice with various annealing cycles between the irradiations and with sequential irradiations performed at different temperatures. Figure 3 shows the O_2 ESD yield vs time for films that were irradiated twice at 20 K. For the first irradiation, the electron dose was small compared to that required to saturate the O_2 ESD yield. Between the first and second irradiation cycles, the sample was annealed to various temperatures. For increasing annealing temperatures, the O_2 yield at the *beginning* of the second irradiation cycle *increases*, which indicates that the intermediate annealing has produced additional precursors *without irradiation*. In fact, the integrated O_2 yield vs annealing temperature in this experiment (data not shown) is similar to the O_2 ESD yield vs irradiation temperature shown in Figure 2. These results suggest that the energetic electrons produce radicals, probably OH, that are immobile in the films at 20 K. Upon heating, the radicals become mobile and react to form the O_2 precursor.

Figure 4 shows the O_2 ESD vs time for a film that was originally irradiated at 100 K and then cooled to 20 K prior to the second irradiation cycle. Also shown is the O_2 ESD from the first irradiation of a film at 20 K. For the film irradiated at 100 K and then irradiated again at 20 K, the O_2 ESD is initially high and decays until the yield approximately follows the yield for a film initially irradiated at 20 K. The difference in the O_2 ESD between the two experiments decays approximately exponentially with time.

Using isotopically layered films of $H_2{}^{16}O$ and $H_2{}^{18}O$ allows one to profile the spatial distribution of the electron-stimulated reactions leading to O_2. A similar approach has been used previously to investigate the ESD of molecular hydrogen with layered films of D_2O and H_2O.[5,6] Figure 5 shows the O_2 ESD vs time for ASW films, where 50 ML of $H_2{}^{16}O$ has been subsequently "capped" with various amounts of $H_2{}^{18}O$. As the amount of $H_2{}^{18}O$ in the cap layer is increased, the $^{16}O_2$ ESD is suppressed (Figure 5). For coverages above ~8 ML, the $^{16}O_2$ ESD is essentially zero. As the irradiations proceed, the layered

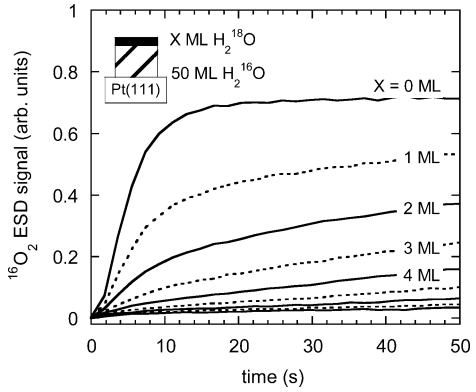

Figure 5. $^{16}O_2$ electron-stimulated desorption vs time from layered films of $H_2{}^{16}O$ and $H_2{}^{18}O$. $H_2{}^{16}O$ ASW films (50 ML) were capped with various amounts of $H_2{}^{18}O$ (from 0 to 8 ML in 1 ML increments). The films were deposited and irradiated at 100 K with 87 eV electrons. The $^{16}O_2$ signal, associated with reactions in the $H_2{}^{16}O$ layer, is suppressed as the $H_2{}^{18}O$ coverage increases. As the irradiation proceeds, electron-induced sputtering and mixing erode the $H_2{}^{18}O$ cap layer and bring $H_2{}^{16}O$ molecules to the surface.

films are mixed and sputtered by the incident electron beam.[20] Therefore, even for relatively large cap layers of $H_2{}^{18}O$, the $^{16}O_2$ signal eventually increases. The 50 ML films are sufficiently thick that electron-stimulated reactions at the Pt/water interface can be neglected. The role of electron-stimulated reactions at the Pt/water interface in the O_2 ESD in thinner films, which is apparent from measurements of the O_2 ESD vs water coverage,[20] will be the subject of a future publication.

For the experiments in Figure 5, the integrated $^{16}O_2$ ESD yield vs $H_2{}^{18}O$ cap layer coverage decays exponentially with a $1/e$ constant of 1.5 ± 0.3 ML (Figure 6, open triangles). These data were integrated over the first ~6 s of irradiation to minimize the influence of the electron-stimulated mixing and sputtering. For longer integration times, the results were qualitatively the same, but the mixing increased the apparent $1/e$ constant. In separate experiments, a 2 ML $H_2{}^{18}O$ layer was deposited at various positions within an $H_2{}^{16}O$ film, and the $^{18}O_2$ and $H_2{}^{18}O$ ESD yields were measured vs the thickness of the $H_2{}^{16}O$ cap layer (Figure 6, circles and solid triangles, respectively). The O_2 ESD signal for both experiments decays with nearly the same exponential constant as the ESD of water. Because water is expected to desorb only from the surface layers,[20] an "ideal"

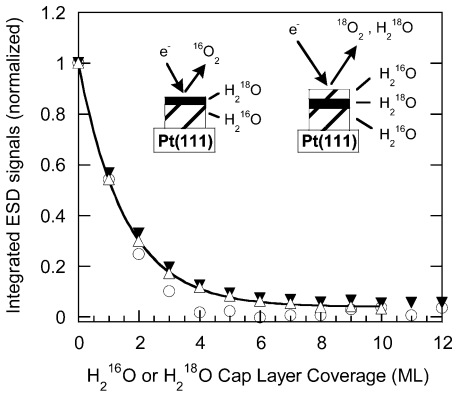

Figure 6. Integrated O_2 and H_2O ESD yields from layered films of $H_2{}^{16}O$ and $H_2{}^{18}O$ vs cap layer coverage. For $H_2{}^{16}O$ capped with $H_2{}^{18}O$, the integrated $^{16}O_2$ ESD (open triangles) decreases exponentially with a constant of 1.7 ML. (The solid line shows the exponential fit to the data.) For films where 2 ML of $H_2{}^{18}O$ was deposited at various locations within 38 ML of $H_2{}^{16}O$, the integrated $^{18}O_2$ and $H_2{}^{18}O$ ESD yields (circles and solid triangles, respectively) also decrease exponentially with similar constants.

capping experiment would presumably give a $1/e$ constant of 1. The fact that the experimental result for the *water* ESD is somewhat larger is probably due to electron-stimulated diffusion and/or roughness in the film that would result in a more diffuse $H_2{}^{16}O/H_2{}^{18}O$ interface, both of which should increase the measured decay constant.

Experiments with layered films of $H_2{}^{16}O$ and $H_2{}^{18}O$ can be used to test if the final precursor contributes one or both of the oxygen atoms in the desorbing O_2. Figure 7a shows the results from experiments where films of $H_2{}^{16}O$ were initially irradiated at 100 K then capped with 2 ML of $H_2{}^{18}O$ and irradiated a second time at 100 K. At the beginning of the second irradiation, only $^{16}O_2$ is produced from the precursors generated during the *first* irradiation, showing that the final precursor donates both O atoms to the desorbing O_2 molecule. As the irradiation proceeds, the $^{16}O^{18}O$ and $^{18}O_2$ increase as the electron-stimulated reactions in the $H_2{}^{18}O$ cap layer proceed.

We have run a series of experiments such as those shown in Figure 7a with various coverages for the $H_2{}^{18}O$ cap layer deposited after the first irradiation. Figure 7b shows the $^{16}O_2$ ESD yield integrated over the first 2 s of the second irradiation vs coverage of the $H_2{}^{18}O$ cap layer (solid circles). For all $H_2{}^{18}O$ cap layer coverages, only $^{16}O_2$ desorbs in any appreciable amount at the beginning of the second irradiation. The integrated yield of $^{16}O_2$ decreases exponentially with increasing cap layer coverage with a $1/e$ constant of $\sim$3 ML.

There are several possible explanations for the results presented in Figures 5−7. One possibility is that only excitations at the ASW/vacuum interface contribute to the production of O_2 even though the typical electron penetration depth, $\sim$10−15 ML at 87 eV, is much longer. However, the O_2 ESD yield vs the total thickness of the film indicates that excitations made within the penetration depth of the incident electrons do contribute to the total yield.[20] Another possible explanation is that, as the cap layer coverage of $H_2{}^{18}O$ increases, $^{16}O_2$ is produced within the buried $H_2{}^{16}O$ layer but is trapped by the cap layer and cannot desorb. This possibility is contradicted by two results: First, very little O_2 desorbs from irradiated films that are subsequently heated to desorb the remaining water and any trapped reaction products (data not shown). Second, for preirradiated films that are subsequently capped and irradiated a second time (Figure 7), O_2 produced deeper in the film *can* desorb during the irradiation. Therefore, the results in Figures 5−7 indicate that the electron-stimulated production of O_2 occurs preferentially at or near the ASW/vacuum interface.

For experiments where an irradiated film is subsequently capped with more water (Figure 7b), the $1/e$ constant of $\sim$3 ML for the O_2 ESD is considerably larger than that obtained in experiments where an $H_2{}^{16}O/H_2{}^{18}O$ layered film was grown and then irradiated ($1/e \sim 1.5$ ML, Figure 6). However, experiments investigating H_2 ESD from layered films of H_2O and D_2O also found a $1/e$ constant of $\sim$2.7 ML. In that case, the H_2 was probably produced by the dissociation of excited water molecules (excitons) at or near the vacuum interface.[6] The similarity of the length scales for H_2 production and O_2 production from preirradiated films suggests that the decay of excitons in the near-surface region might also initiate the last nonthermal reaction that produces O_2. The shorter length scale, $1/e \sim 1.5$ ML, for O_2 ESD from $H_2{}^{16}O/H_2{}^{18}O$ layered films probably reflects the spatial profile of the final O_2 precursor in the film and suggests that the reactions *leading* to the final O_2 precursor occur at the surface, probably because the OH radicals segregate there.[21,22] Finally, because the first irradiation creates the precursors at or near the vacuum interface of the $H_2{}^{16}O$ film, the suppression of the initial O_2 yield during the second irradiation by the $H_2{}^{18}O$ cap layer also shows that the final precursor does not diffuse to the surface of the film at 100 K.

Previous research[11,12] suggested that the final O_2 precursor may be HO_2 or H_2O_2, or both, and the results in Figure 7 are consistent with this. To test H_2O_2 as a possible precursor, we investigated the O_2 ESD from water films dosed with H_2O_2 in various amounts and deposition sequences. Figure 8 shows the O_2 ESD vs irradiation time for relatively thick H_2O films that are capped with $H_2O + H_2O_2$ mixtures and irradiated at various temperatures. For comparison, the O_2 ESD from neat H_2O films is also shown for 25 and 100 K. A significant enhancement of O_2 ESD for the H_2O_2-dosed samples is observed at all irradiation temperatures. The O_2 ESD yield rapidly increases on a time scale that is short compared to the time for the O_2 ESD to reach saturation in the neat water film, goes through a maximum, and then decays to the steady-state value for pure water films at longer irradiation times. The difference between the integrated O_2 ESD vs time for the H_2O_2-dosed and pure H_2O samples (i.e., the additional O_2 ESD due to the H_2O_2) is approximately the same at all temperatures.

For H_2O_2-dosed films that are subsequently capped with more water, the enhanced O_2 ESD yield observed at the beginning of the irradiation decreases exponentially as the water cap layer coverage increases with a $1/e$ constant of $\sim$3 ML (Figure 7b). In addition, the O_2 ESD yield from H_2O_2-dosed films vs temperature (data not shown) is qualitatively similar to that for neat water (Figure 2). Therefore, all the observations are consistent with H_2O_2 being one of the precursors for the O_2 ESD. However, the experiments also indicate that H_2O_2 is not the *final* precursor. In particular, the O_2 ESD signal from H_2O_2-dosed films is initially zero and increases as $\sim(1 - e^{-\alpha t})$ at early times for all temperatures, indicating that further reactions to produce HO_2 are required prior to the formation of O_2. (The kinetic modeling discussed below supports this conclusion.) HO_2 is also consistent with previous investigations where optical absorption spectroscopy and EPR reveal four major radiolysis products trapped in bulk irradiated ice: H, OH, HO_2, and electrons.[23−25] However, at 77 K, only OH and trapped electrons are detected in the irradiated bulk ices, and they decay with rather complicate kinetics, primarily between 90 and 140 K.[24] As OH decays with increasing temperature, HO_2 radicals appear.[24]

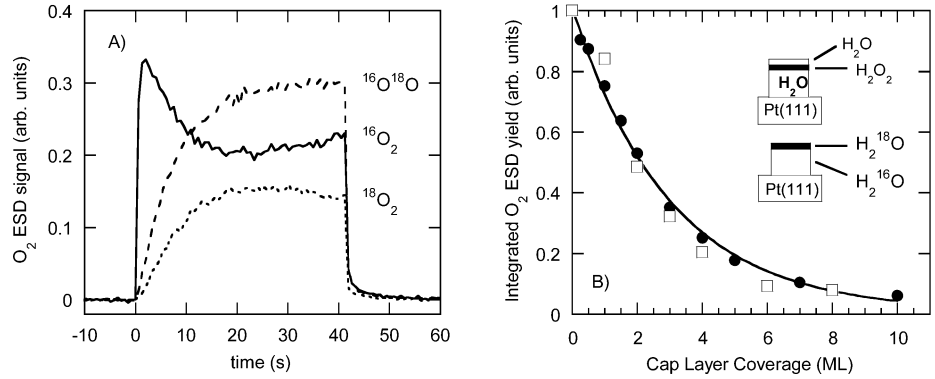

Figure 7. (A) O_2 electron-stimulated desorption vs time. $H_2{}^{16}O$ films (20 ML) were deposited at 100 K on Pt(111) and irradiated for 40 s. After the irradiation, 2 ML of $H_2{}^{18}O$ was deposited on top and a second 40 s irradiation cycle was performed at 100 K, monitoring $^{16}O_2$ (solid line), $^{16}O^{18}O$ (dashed line), and $^{18}O_2$ (dotted line). (B) Integrated O_2 ESD yields vs cap layer coverage. For a 20 ML $H_2{}^{16}O$ film irradiated and then capped with various amounts of $H_2{}^{18}O$ and irradiated a second time (all at 100 K), the initial $^{16}O_2$ ESD yield, integrated over the first ~2 s of the irradiation, decreases exponentially with a $1/e$ constant of ~3 ML (solid circles). For an H_2O film (82 ML) dosed with a layer of H_2O and H_2O_2 at various locations, the initial O_2 ESD yield also decreases exponentially as the H_2O cap layer coverage increases (open squares) with approximately the same length scale.

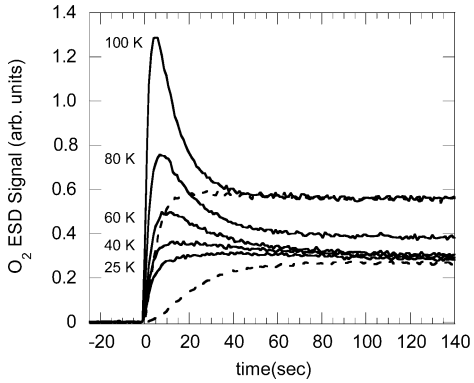

Figure 8. O_2 electron-stimulated desorption vs time. H_2O films (80 ML) were deposited at 120 K, capped with an $H_2O_2-H_2O$ layer, and then irradiated at various temperatures (solid lines). The O_2 ESD from pure 80 ML H_2O films irradiated at 25 and 100 K (dotted lines) are also shown. For the H_2O_2-dosed films, the O_2 ESD is initially enhanced compared to the pure water films.

IV. Discussion

A. O_2 Electron-Stimulated Reaction Scheme. On the basis of prior research, the results presented above, and the kinetic modeling discussed below, we believe the following reactions account for most of the electron-stimulated production of O_2 in thin ASW films:

$$e^- + H_2O_{bulk} \rightarrow H_2O^+ + 2e^- \quad (1)$$

$$H_2O^+ + e^- \rightarrow H_2O^*{}_{bulk} \quad (2)$$

$$H_2O^*{}_{bulk} \rightarrow H_2O^*{}_{vac} \quad (3)$$

$$H_2O^*{}_{vac} \rightarrow H_{des} + OH_{vac} \quad (4)$$

$$OH_{vac} + OH_{vac} \overset{k_2,k_3}{\rightleftharpoons} H_2O_{2(vac)} \quad (5)$$

$$H_2O_{2(vac)} + OH_{vac} \xrightarrow{k_4} HO_{2(vac)} + H_2O \quad (6)$$

$$HO_{2(vac)} + A^* \xrightarrow{k_5} O_2 + \text{other products} \quad (7)$$

where the subscripts "bulk" and "vac" denote species located in the bulk of the ASW film and at (or near) the ASW/vacuum interface, respectively. The reaction rate constants k_2 through k_5 for reactions 5−7 will be used to fit the kinetic model to the data. In reaction 5, k_2 and k_3 are for the forward and backward reactions, respectively.

The first four reactions are suggested by previous investigations of the electron-stimulated production of H, H_2, O, and O_2. The O_2 ESD has an energetic threshold at ~9 eV and the yield increases monotonically with incident electron energy,[12,26] indicating that the first step in O_2 ESD is predominantly ionization (reaction 1). Because the mean penetration depth for ~100 eV electrons is approximately 3 nm (i.e., ~10−15 ML), most of the ionizations occur in the bulk and not at the vacuum interface of the film.[27] For the electron-stimulated production of H, O, and H_2, the next step appears to be electron−ion recombination to form a mobile, electronically excited neutral water molecule, an exciton (reaction 2).[2,5,6,20,28] The O_2 ESD vs coverage for very thin films (i.e., coverages less than 10 ML)[29] also indicates that electron−ion recombination is important.

In the gas phase, electronically excited water dissociates to H + OH, H_2 + O, or 2H + O. The branching ratio depends on the excitation energy, but typically, $H_2O^* \rightarrow H + OH$ accounts for more than 50%.[30,31] In thin ASW films, the electronically excited water molecules typically do not dissociate in the bulk (at least under low-current/low-energy electron irradiation). Instead, the excitons migrate to (reaction 3), and preferentially dissociate at or near, the water/vacuum or water/Pt interface.[5,6,28] Recent coupled-cluster calculations indicate that the lowest excited singlet and triplet states of hydrogen-bonded water molecules are each nondissociative for stretching of an OH bond.[32] This may inhibit the exciton from dissociating in the bulk in favor of dissociation at the surface on dangling OH groups, consistent with the experimental observations. For excitons that dissociate at the vacuum interface, H atoms are one of the dominant products.[2] In addition, the electron-stimulated production of H^+ and H^-,[4,7] which should occur preferentially at the vacuum interface, also lead to the formation of OH.[14] Therefore, previous results strongly suggest that OH radicals are produced at or near the vacuum interface of electron-irradiated thin water films (reaction 4), consistent with the results of Figures 5 and 6.

At the vacuum interface, the OH radicals can react to form H_2O_2 (reaction 5). H_2O_2 also reacts with OH to produce HO_2 (reaction 6). Reactions 5 and 6 are both known from previous investigations of the radiation chemistry in liquid water and ice.[24,33,34] Finally, the data presented above suggest that the O_2

that desorbs is produced in a nonthermal reaction involving the HO_2 (reaction 7). Because both O atoms in the O_2 come from the same precursor molecule, one possibility is that an energetic electron directly dissociates an HO_2 into O_2 and H. Alternatively, the HO_2 might react with some other short-lived species in the film. For example, HO_2 might react with a nonthermal OH produced from the dissociation of a nearby water molecule. (Because the reaction partner, if any, for the HO_2 is unknown, we designate it as A^* in reaction 7.)

Instead of excitons migrating to the vacuum interface and dissociating to produce OH radicals, another possibility is that ionization in the bulk is followed by rapid proton transfer to form H_3O^+ and OH. The OH could then diffuse to, and trap at, the water/vacuum interface. In that case, reactions 5−7 could proceed as already discussed. This model, which appears to be consistent with the O_2 data presented here, does not explain the electron-stimulated production of H, O, and H_2 at the vacuum interface.[2,5,6,28] In contrast, exciton dissociation at or near the vacuum interface naturally accounts for all these processes. However, we believe that diffusion of OH radicals through ASW films is important for films thin enough that reactions at the water/Pt interface need to be considered (data not shown).

B. Kinetic Modeling. The data can be qualitatively reproduced with a kinetic model based on the reaction scheme discussed above. To keep the model tractable and to reduce the number of free parameters involved, we treat reactions 1 through 4 as a single "reaction" that produces OH radicals at the vacuum interface of the films:

$$e^- + H_2O \xrightarrow{k_1} OH_{vac} + e^- + H \qquad (8)$$

The influence of ionization (reaction 1), electron−ion recombination (reaction 2), exciton migration (reaction 3), and dissociation (reaction 4) will thus be reflected in the rate constant, k_1, for reaction 8. The system of linear differential equations representing reactions 5−8 (see Appendix) was numerically integrated to find the concentrations of OH, H_2O_2, and HO_2 vs irradiation time. The kinetic modeling assumes that the reactions are spatially homogeneous, whereas the actual reactions apparently occur in a thin layer near the vacuum interface (i.e., very inhomogeneous). However, it seems plausible to model the experiments as homogeneous reactions in a thin, approximately two-dimensional, layer near the vacuum interface. Therefore, the concentrations for various species are specified by their areal density (i.e., particles/cm^2).

The measured O_2 ESD vs time is proportional to the rate at which O_2 is produced, which is proportional to the HO_2 concentration times a concentration of excitations (or excitation products) generated by the incident electron beam. To determine the rate constants, it is necessary to experimentally determine the absolute rate at which O_2 is produced, or alternatively, the concentration of at least one of the reactants or products in the model. The experiments on the H_2O_2 predosed films are well suited for this because, for a known initial concentration of H_2O_2, the kinetic model predicts the amount of extra O_2 ESD that should be produced compared to a pure water film. As discussed in the Appendix, the initial concentration of H_2O_2 can be estimated in two different ways. The rate constants, $k_1(T)-k_5(T)$, can then be found by fitting the model to the data for the experiments for (i) pure water films, (ii) for films initially irradiated at 100 K and subsequently irradiated at lower temperatures, and (iii) H_2O_2 predosed films. The values extracted for the rate constants using this approach are given in Table A1 in the Appendix.

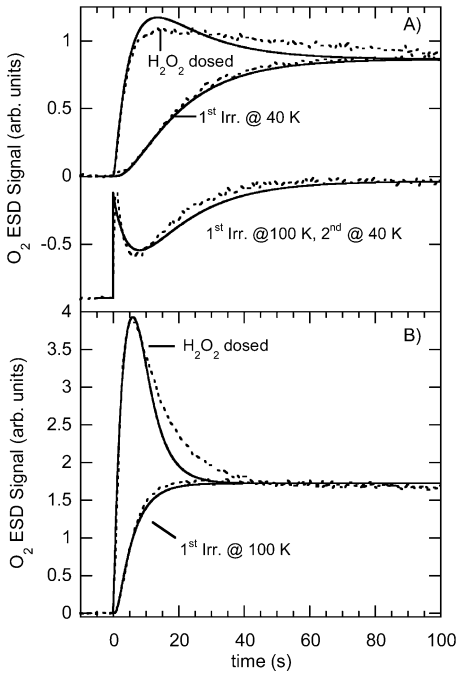

Figure 9. O_2 electron-stimulated desorption vs time. The results of the kinetic model (solid lines) are compared to experimental results (dotted lines). (A) Three experiments are shown: (i) pure ASW film irradiated for the first time at 40 K, (ii) film initially irradiated at 100 K and then subsequently irradiated at 40 K, and (iii) an H_2O film capped with an $H_2O_2-H_2O$ layer and irradiated at 40 K. (B) Two experiments are shown: (i) a pure ASW film irradiated for the first time at 100 K, (ii) an H_2O film capped with an $H_2O_2-H_2O$ layer and irradiated at 100 K. In all cases, the model semiquantitatively reproduces the data.

Figure 9a shows examples of the kinetic model compared to data for irradiations performed at 40 K. The three experiments correspond to a pure water film irradiated for the first time, a film that was first irradiated at 100 K and then irradiated a second time at 40 K, and a film that was predosed with H_2O_2 prior to irradiation. For the pure film irradiated the first time, the initial concentrations of OH, H_2O_2, and HO_2 were all set to zero in the kinetic model. For the H_2O_2 predosed film, the initial concentration of H_2O_2 was set to 1.5×10^{14} H_2O_2/cm^2. For the film preirradiated at 100 K, the initial concentrations of OH, H_2O_2, and HO_2 were 3×10^{12} cm^{-2}, 6×10^{12} cm^{-2}, and 1.5×10^{13} cm^{-2}, respectively, which correspond to 65% of the steady-state concentrations calculated for a pure film irradiated at 100 K. For all three experiments, the model qualitatively reproduces the data.

Figure 9b shows the model results for irradiations at 100 K corresponding to the pure films and the H_2O_2 predosed films. For the H_2O_2 predosed film, the initial concentration of H_2O_2 was set to 1.6×10^{14} H_2O_2/cm^2. Again, the model reproduces the data reasonably well. In fact, a consistent set of model parameters (i.e., constants k_1-k_5) can nearly quantitatively reproduce the O_2 ESD data for pure water films irradiated over the entire temperature range (e.g., fit all the data in Figure 1). With the same set of parameters and the appropriate initial concentrations for OH, H_2O_2, and HO_2 described above, the model can also qualitatively fit all the data for films initially irradiated at 100 K and subsequently irradiated a second time at lower temperatures (e.g., Figure 4), and for films predosed with H_2O_2 (e.g., Figure 8).

Qualitatively, $k_1(T)$, $k_2(T)$, $k_4(T)$, and $k_5(T)$ are approximately constant for temperatures below ~80−100 K and increasing at higher temperatures. The observation that the electron-stimulated reactions leading to O_2 occur even at low temperatures is not

surprising given the amount of energy deposited into the film by the incident electrons. However, the increase in the rate constants k_1, k_2, k_4, and k_5 above ~80 K suggests that thermal effects begin to enhance the nonthermal reactions in this regime. There are probably several different effects that account for the temperature dependence of the various reactions. For example, because both $k_2(T)$ and $k_4(T)$ should be related to the mobility of the OH radicals in the film, which should be enhanced at higher temperatures, $k_2(T)$ and $k_4(T)$ are expected to increase. As discussed above, several different processes are responsible for the creation of OH radicals at the vacuum interface. Therefore, assigning the temperature dependence of k_1 to any particular step is difficult. One possible explanation for the increase of both k_1 and k_5 above ~80 K is that more excitons reach the surface at higher temperature, perhaps due to higher mobility. Other possibilities include enhanced electron−ion recombination at high temperatures[28] and temperature-dependent changes in the structure of water near the surface.[12] To fit the data, the back reaction to form two OH's from H_2O_2 (reaction 5) is necessary, particularly at higher temperatures. However, $k_3(T)$ seems to be only weakly dependent on the temperature, suggesting it is due to the dissociation of H_2O_2 by energetic electrons or excitons.

The model predicts the concentrations of OH, H_2O_2, and HO_2 vs time. Above ~80 K, the concentrations of H_2O_2 and HO_2 at steady state are $\sim 1-3 \times 10^{13}$ cm^{-2} (i.e., ~1−3% relative to the amount of water in a monolayer), and the OH concentrations are lower. At lower temperatures, the model predicts that the concentration of H_2O_2 increases, while the concentration of HO_2 decreases. Qualitatively, the relatively low concentrations are consistent with previous observations.[14] For example, the electron-stimulated desorption of both H_2O and H_2, which should reflect the concentration of water in the surface layer, are approximately independent of time during the time in which the O_2 ESD signal is coming to steady state.[6,20]

The rate constant k_1 gives the rate at which OH radicals are produced at or near the vacuum interface. According to the model results, $\sim 9 \times 10^{12}$ OH/cm^2 s are produced at 100 K. For the corresponding experiments, the incident electron flux was $\sim 2.5 \times 10^{13}$ e$^-$/cm^2, which indicates that ~1 OH radical is produced per 3 electrons. Because it takes 3 OH's to produce one oxygen molecule, this corresponds to ~1 O_2 per 10 electrons. Given the approximations and uncertainties in the model and data, this is in reasonable agreement with previous measurements of the electron-stimulated sputtering where the *total* sputtering yield at 100 K was ~1 H_2O per incident electron with O_2 ESD accounting for (at most) $^1/_3$ of that yield.[20]

A number of other reactions in addition to those discussed above are known or believed to occur during radiolysis of liquid water and ice, some of which can contribute to the O_2 produced in the present experiments.[33,34] For example, the reaction

$$OH + HO_2 \rightarrow O_2 + H_2O \qquad (9)$$

is believed to be responsible for some of the O_2 produced in the radiolysis of liquid water, and the rate constant for this reaction is larger than that for reaction 6 in liquid water.[35] Because OH and HO_2 are both present in the electron-irradiated ices, we might expect reaction 9 to contribute to the O_2 production. However, for the experiments where a water film was irradiated at low temperature and then annealed to a higher temperature (Figure 3), no appreciable O_2 production was detected *during* the annealing cycle, even though reactions 5 and 6 to produce H_2O_2 and HO_2 occurred. This result suggests that reaction 9 is a minor channel in the present experiments. In general, the experimental results in conjunction with the kinetic modeling suggest that reactions 1−7 are responsible for the majority of the O_2 ESD that is observed.

The electron-stimulated reactions leading to O_2 appear to be primarily nonthermal. For example, in Figure 1, the O_2 ESD signal quickly decays to zero at all temperatures once the electron beam is turned off, suggesting that the last reaction to produce O_2 involves either the incident electrons directly or some short-lived, nonthermal reaction products, perhaps from the decay of the excitons at or near the vacuum interface (reaction 7). The possibility that the last reaction is a fast thermal reaction is ruled out by the observation that, for any irradiation temperature from 20 to 130 K, if an irradiation is interrupted for some time and then resumed (isothermally), the O_2 ESD signal promptly returns to the value it had when the irradiation was stopped (i.e., on time scale that is short compared to the time to reach saturation during the *initial* irradiation). If the last reaction were thermal, the decay of the signal at the end of the irradiation would be due to the depletion of the final precursor.

The prompt recovery of the O_2 ESD signal suggests that the distribution of *all* the O_2 precursors did not change appreciably when the electron beam was off. Therefore, either the reaction rates were small when the electron beam was off, or the concentrations of OH and H_2O_2 are sufficiently low during irradiation that no more HO_2 can be produced once the electron beam is shut off (thus keeping distribution of precursors unchanged). However, the increased O_2 ESD yield for films irradiated at 20 K, annealed to higher temperature and then irradiated a second time (Figure 3), shows that the reactions to produce the final precursor (reactions 5 and 6) can proceed thermally *and* that the concentrations of OH and H_2O_2 are not negligible during irradiation, at least at low temperatures. A model in which the reaction rate is substantially increased when the electron beam is on can reconcile these observations. For films initially irradiated at 100 K and subsequently irradiated at lower temperature (e.g., Figure 4), the kinetic modeling indicates that the concentrations of OH and H_2O_2 need to be smaller than the HO_2 concentration to account for the data. The kinetic model predicts that the OH concentration at steady state is lower than the HO_2 concentration at all temperatures and that the H_2O_2 steady-state concentration substantially decreases compared to the HO_2 concentration as the temperature increases.

V. Conclusions

In summary, experiments using isotopically labeled films of D_2O, $H_2{}^{16}O$, and $H_2{}^{18}O$ demonstrate that the low-energy, electron-stimulated production of molecular oxygen in ASW films occurs predominantly at the ASW/vacuum interface from a stable precursor, most likely HO_2. The final precursor for O_2 is not a primary product of water molecule radiolysis, but the result of several intermediate reactions between OH radicals. A kinetic model of the nonthermal reactions qualitatively reproduces all the features of the electron-stimulated reactions over a wide temperature range.

Acknowledgment. This work was supported by the U.S. Department of Energy, Office of Basic Energy Sciences, Chemical Sciences Division. Experiments were performed in the Environmental Molecular Sciences Laboratory, a national scientific user facility sponsored by the Department of Energy's Office of Biological and Environmental Research and located at Pacific Northwest National Laboratory which is operated for

the U.S. Department of Energy by Battelle Memorial Institute under Contract No. DE-AC06-76RLO 1830.

Appendix

The differential equations used to model the O_2 ESD kinetics are:

$$\frac{d[OH]}{dt} = k_1 + 2k_3[H_2O_2] - k_2[OH]^2 - k_4[OH][H_2O_2] \quad (A1)$$

$$\frac{d[H_2O_2]}{dt} = k_2[OH]^2 - k_3[H_2O_2] - k_4[OH][H_2O_2] \quad (A2)$$

$$\frac{d[HO_2]}{dt} = k_4[OH][H_2O_2] - k_5[HO_2] \quad (A3)$$

where [OH], [H_2O_2], and [HO_2] are the concentrations of OH, H_2O_2, and HO_2 as a function of time, respectively. As discussed in the text, to match the experimental results, all the rate constants, k_1 through k_5, are assumed to be proportional to the incident electron current (i.e., they are zero, or at least significantly reduced when the electron beam is off). In equation A1, the first source term for OH should be proportional to the concentration of water in the bulk. However, this is assumed to be constant and is absorbed into the rate constant, k_1. The O_2 ESD signal vs time, Y_{O_2}, is proportional to the concentration of HO_2 and the reaction partner A^* which, as discussed in the text, could be the energetic electrons themselves or some short-lived electron-stimulated reaction product:

$$Y_{O_2}(t) = \alpha k_5[A^*][HO_2] \quad (A4)$$

where α is a constant related to (among other things) the O_2 detection efficiency in the quadrupole mass spectrometer. Because [A^*] is assumed to be proportional to the electron flux and independent of time when the beam is on (i.e., [A^*] = constant or 0 when the electron beam is on or off, respectively), it can be absorbed into rate constant k_5:

$$Y_{O_2}(t) = \alpha k_5[HO_2] \quad (A5)$$

It is easy to show from equations A1−A3 that the "normalized" concentrations [OH](t)/k_1, [H_2O_2](t)/k_1, [HO_2](t)/k_1, and $Y_{O_2}(t)/k_1$ are independent of the value of k_1 so long as the constants k_2 and k_4 are scaled appropriately: $k_2 = a/k_1$ and $k_4 = b/k_1$ (where a and b are constants). Therefore, it is not possible to determine a unique set of rate constants by comparing the model to the data if one knows only the *relative* rate at which O_2 is produced in the experiments. To determine the rate constants, one needs to know the absolute rate at which O_2 is produced or the concentration of one of the species (OH, H_2O_2, or HO_2) at some point in the experiment. The initial coverage of H_2O_2 in the experiments on the H_2O_2 predosed films (e.g., Figure 8) can be estimated in two ways. First, predosing with H_2O_2 increases the total integrated O_2 ESD relative to the pure water films. If all the H_2O_2 is eventually converted into O_2, as assumed in the model, then the extra O_2 ESD can be used to estimate the amount of H_2O_2 originally dosed into the films. Experimentally, we find that the extra O_2 ESD from the H_2O_2 predosed films is approximately independent of temperature; it decreases by only ~30% as the temperature decreases from 130 to 25 K. From the integral of the additional O_2, we estimate that the initial coverage of H_2O_2 was ~0.09−0.14 ML (relative to a water ML), corresponding to ~9×10^{13} to 1.4×10^{14} H_2O_2/cm^2.

TABLE A1: Rate Constants for Reactions 5−8 Obtained by Fitting to the O_2 ESD vs Time

temperature (K)	k_1 (cm^{-2} s^{-1})	k_2 (cm^2 s^{-1})	k_3 (s^{-1})	k_4 (cm^2 s^{-1})	k_5 (s^{-1})
20	5×10^{12}	1.5×10^{-13}	0.02	6×10^{-15}	0.2
40	5×10^{12}	1.5×10^{-13}	0.02	7×10^{-15}	0.2
60	5×10^{12}	2×10^{-13}	0.02	1.2×10^{-14}	0.2
80	7×10^{12}	2×10^{-13}	0.04	2×10^{-14}	0.2
90	8×10^{12}	2×10^{-13}	0.04	4×10^{-14}	0.2
100	9×10^{12}	2×10^{-13}	0.05	1×10^{-13}	0.2
110	1.1×10^{13}	8×10^{-13}	0.07	2×10^{-13}	0.35
120	1.3×10^{13}	1×10^{-12}	0.07	5×10^{-13}	0.5
130	1.55×10^{13}	2×10^{-12}	0.07	6×10^{-13}	0.75

The second method to estimate the H_2O_2 coverage is based on temperature-programmed desorption of unirradiated H_2O_2 predosed films. As the films are heated, the water preferentially desorbs, and eventually, the $H_2O-H_2O_2$ solution reacts with the Pt(111) surface to form a H_2O-OH layer, which desorbs at a significantly higher temperature than a pure water monolayer.[36] The integrated area of this high-temperature peak is proportional to the initial H_2O_2 coverage. With this method, we estimate that the initial coverage of H_2O_2 was ~1.7×10^{14} to 2.0×10^{14} H_2O_2/cm^2, which is in reasonable agreement with the first estimate. Therefore, we use an initial concentration of ~1.5×10^{14} H_2O_2/cm^2 in the kinetic modeling for the H_2O_2 predosed experiments.

Table A1 lists the rate constants obtained by fitting the O_2 ESD data as described above. The kinetic model assumes a homogeneous two-dimensional system, and the units for the rate constants reflect this assumption. However, in the experiments, the reactions apparently occur in a thin region at or near the ASW/vacuum interface, and the concentrations of various species are probably nonuniform in the direction normal to the interface.

References and Notes

(1) *Radiation Chemistry: Principles and Applications*; Farhataziz, Rodgers, M. A. J., Eds.; VCH Publishers: New York, 1987; p 641.
(2) Kimmel, G. A.; Orlando, T. M. *Phys. Rev. Lett.* **1995**, *75*, 2606.
(3) Kimmel, G. A.; Orlando, T. M. *Phys. Rev. Lett.* **1996**, *77*, 3983.
(4) Noell, J. O.; Melius, C. F.; Stulen, R. H. *Surf. Sci.* **1985**, *157*, 119.
(5) Petrik, N. G.; Kimmel, G. A. *Phys. Rev. Lett.* **2003**, *90*, 166102.
(6) Petrik, N. G.; Kimmel, G. A. *J. Chem. Phys.* **2004**, *121*, 3736.
(7) Rowntree, P.; Parenteau, L.; Sanche, L. *J. Chem. Phys.* **1991**, *94*, 8570.
(8) Westley, M. S.; Baragiola, R. A.; Johnson, R. E.; Baratta, G. A. *Nature* **1995**, *373*, 405.
(9) Westley, M. S.; Baragiola, R. A.; Johnson, R. E.; Baratta, G. A. *Planet. Space Sci.* **1995**, *43*, 1311.
(10) Brown, W. L.; Lanzerotti, L. J.; Johnson, R. E. *Science* **1982**, *218*, 525.
(11) Sieger, M. T.; Simpson, W. C.; Orlando, T. M. *Nature* **1998**, *394*, 554.
(12) Orlando, T. M.; Sieger, M. T. *Surf. Sci.* **2003**, *528*, 1.
(13) Baragiola, R. A.; Vidal, R. A.; Svendsen, W.; Schou, J.; Shi, M.; Bahr, D. A.; Atteberrry, C. L. *Nuclear Instruments and Methods in Physics Research, Section B: Beam Interactions with Materials and Atoms* **2003**, *209*, 294.
(14) Pan, X.; Bass, A. D.; Jay-Gerin, J. P.; Sanche, L. *Icarus* **2004**, *172*, 521.
(15) Yates, J. T. *Experimental Innovations in Surface Science: A Guide to Practical Laboratory Methods and Instruments*; Springer-Verlag New York, Inc.: New York, 1998.
(16) Dohnalek, Z.; Kimmel, G. A.; Ayotte, P.; Smith, R. S.; Kay, B. D. *J. Chem. Phys.* **2003**, *118*, 364.
(17) Kimmel, G. A.; Stevenson, K. P.; Dohnalek, Z.; Smith, R. S.; Kay, B. D. *J. Chem. Phys.* **2001**, *114*, 5284.
(18) Stevenson, K. P.; Kimmel, G. A.; Dohnalek, Z.; Smith, R. S.; Kay, B. D. *Science* **1999**, *283*, 1505.
(19) Manatt, S. L.; Manatt, M. R. R. *Chem.−Eur. J.* **2004**, *10*, 6540.
(20) Petrik, N. G.; Kimmel, G. A. *J. Chem. Phys.* **2005**, *123*, 054702.

(21) Belair, S. D.; Hernandez, H.; Francisco, J. S. *J. Am. Chem. Soc.* **2004**, *126*, 3024.
(22) Roeselova, M.; Vieceli, J.; Dang, L. X.; Garrett, B. C.; Tobias, D. J. *J. Am. Chem. Soc.* **2004**, *126*, 16308.
(23) Ershov, B. G.; Pikaev, A. K. *Radiat. Res. Rev.* **1969**, *2*, 1.
(24) Kevan, L. Radiation Chemistry of Frozen Polar Systems. In *Actions Chimiques et Biologiques des Radiations*; Haïssinsky, M., Ed.; Masson: Paris, 1969; Vol. 13, p 57.
(25) Plonka, A.; Szajdzinska-Pietek, E.; Bednarek, J.; Hallbrucker, A.; Mayer, E. *Phys. Chem. Chem. Phys.* **2000**, *2*, 1587.
(26) Petrik, N. G.; Kimmel, G. A. *J. Phys. Chem. B* **2005**, *109*, 15835.
(27) Laverne, J. A.; Pimblott, S. M. *J. Phys. Chem. A* **1997**, *101*, 4504.
(28) Orlando, T. M.; Kimmel, G. A. *Surf. Sci.* **1997**, *390*, 79.
(29) Petrik, N. G.; Kimmel, G. A. *J. Chem. Phys.* **2004**, *121*, 3727.
(30) Pimblott, S. M.; Mozumder, A. Modeling of Physicochemical and Chemical Processes in the Interactions of Fast Charged Particles with Matter. In *Charged Particles and Photon Interactions with Matter*; Mozumder, A., Hatano, Y., Eds.; Marcel Dekker: New York, Basel, 2004; p 75.
(31) Rowe, B. R.; Vallee, F.; Queffelec, J. L.; Gomet, J. C.; Morlais, M. *J. Chem. Phys.* **1988**, *88*, 845.
(32) Chipman, D. M. *J. Chem. Phys.* **2005**, *122*, 044111.
(33) Buxton, G. V. The Radiation Chemistry of Liquid Water: Principles and Applications. In *Charged Particles and Photon Interactions with Matter*; Mozumder, A., Hatano, Y., Eds.; Marcel Dekker: New York, Basel, 2004; p 331.
(34) Garrett, B. C.; Dixon, D. A.; Camaioni, D. M.; Chipman, D. M.; Johnson, M. A.; Jonah, C. D.; Kimmel, G. A.; Miller, J. H.; Rescigno, T. N.; Rossky, P. J.; Xantheas, S. S.; Colson, S. D.; Laufer, A. H.; Ray, D.; Barbara, P. F.; Bartels, D. M.; Becker, K. H.; Bowen, H.; Bradforth, S. E.; Carmichael, I.; Coe, J. V.; Corrales, L. R.; Cowin, J. P.; Dupuis, M.; Eisenthal, K. B.; Franz, J. A.; Gutowski, M. S.; Jordan, K. D.; Kay, B. D.; LaVerne, J. A.; Lymar, S. V.; Madey, T. E.; McCurdy, C. W.; Meisel, D.; Mukamel, S.; Nilsson, A. R.; Orlando, T. M.; Petrik, N. G.; Pimblott, S. M.; Rustad, J. R.; Schenter, G. K.; Singer, S. J.; Tokmakoff, A.; Wang, L. S.; Wittig, C.; Zwier, T. S. *Chem. Rev.* **2005**, *105*, 355.
(35) Frongillo, Y.; Goulet, T.; Fraser, M. J.; Cobut, V.; Patau, J. P.; Jay-Gerin, J. P. *Radiat. Phys. Chem.* **1998**, *51*, 245.
(36) Clay, C.; Haq, S.; Hodgson, A. *Phys. Rev. Lett.* **2004**, *92*.